

## XMM-NEWTON OBSERVATION OF THE NARROW-LINE QSO PHL 1092: DETECTION OF A HIGH AND VARIABLE SOFT COMPONENT

SURAJIT DASGUPTA<sup>1</sup>, A. R. RAO<sup>1</sup>, G. C. DEWANGAN<sup>2</sup>

*Draft version November 4, 2018*

### ABSTRACT

We present results based on an XMM-Newton observation of the high luminosity narrow-line QSO PHL 1092 performed in 2003 January. The 0.3 – 10 keV spectrum is well described by a model which includes a power-law ( $\Gamma \sim 2.1$ ) and two blackbody components ( $kT \sim 130$  eV and  $kT \sim 50$  eV). The soft X-ray excess emission is featureless and contributes  $\sim 80\%$  to the total X-ray emission in the 0.3 – 10 keV band. The most remarkable feature of the present observation is the detection of X-ray variability at very short time scale: the X-ray emission varied by 35% in about 5000 s. We find that this variability can be explained by assuming that only the overall normalization varied during the observation. There was no evidence for any short term spectral variability and the spectral shape was similar even during the *ASCA* observation carried out in 1997. Considering the high intrinsic luminosity ( $\sim 2 \times 10^{45}$  erg s $^{-1}$ ) and the large inferred mass of the putative black hole ( $\sim 1.6 \times 10^8 M_{\odot}$ ), the observed time scale of variability indicates emission at close to Eddington luminosity arising from very close to the black hole. We suggest that PHL 1092 in particular (and narrow line Seyfert galaxies in general) is a fast rotating black hole emitting close to its Eddington luminosity and the X-ray emission corresponds to the high-soft state seen in Galactic black hole sources.

*Subject headings:* galaxies: active — galaxies: individual (PHL 1092) — X-rays: galaxies

### 1. INTRODUCTION

Narrow Line Seyfert 1 (NLS1) galaxies were first classified as a subclass of Seyfert 1 by Osterbrock & Pogge (1985) on the basis that the FWHM of  $H_{\beta}$  line is less than 2000 km s $^{-1}$ , the ratio of  $[\text{O III}]\lambda 5007$  to  $H_{\beta}$  is less than 3, and they often show strong Fe II emission in 4500 – 4680 Å and 5105 – 5395 Å regions. Though NLS1s are identified by their optical properties they have even more remarkable properties in the X-ray band as compared to other Seyfert galaxies. They show evidence for strong excess of soft X-rays (dominant below  $\sim 2$  keV) above the hard X-ray continuum extrapolation and rapid X-ray variability (doubling times of minutes to hours).

Soft X-ray excess emission above a power-law continuum is usually identified as the steepening of the X-ray continuum below  $\sim 2$  keV. This soft excess emission was first observed by *HEAO-1* (Pravdo et al. 1981) and *EXOSAT* (Arnaud et al. 1985; Singh et al. 1985). Boller et al. (1996) showed that AGN with steepest soft X-ray spectra in the *ROSAT* band tend to lie at the lower end of the  $H_{\beta}$  line width distribution and hence AGNs with soft excess emission are predominantly NLS1 galaxies. Detailed X-ray study of NLS1s was carried out with *ASCA* which confirmed the soft X-ray emission and, in addition, showed that the 2 – 10 keV continuum slope too is steeper and anti-correlated with the FWHM of the  $H_{\beta}$  line (Brandt et al. 1997; Leighly 1999b; Vaughan et al. 1999). *ASCA* observations also showed that many NLS1s have Fe K $\alpha$  line arising from highly ionized iron, and hence the accretion disks of NLS1s must be ionized (Dewangan 2002; Porquet et.al. 2004; Ballantyne et al.

2001). NLS1s are the most extreme X-ray variable objects among the radio-quiet AGNs. NLS1s frequently exhibit rapid (doubling time scale of a few hundred seconds) and/or large (up to a factor of 100) amplitude X-ray variability (Boller et al. 1996; Dewangan et al. 2001, 2002). The excess variance for NLS1s is typically an order of magnitude higher than that observed for Broad Line Seyfert 1's (BLS1).

There are high-luminosity analogs of this class, the prototype of which is I Zw 1 (Phillips 1976). I Zw 1 also has weak forbidden lines, narrow permitted lines, and strong Fe II lines. One of the most extreme narrow line Fe II QSO is PHL 1092 (B=16.7, z=0.396) (Bergeron & Kunth 1980, 1984; Kwan et. al. 1995). Its Fe II $\lambda 4570/H_{\beta}$  ratio is 5.3, and its  $H_{\beta}$  line width is 1800 km s $^{-1}$  (Bergeron & Kunth 1984). PHL 1092 was rapidly variable during a *ROSAT* observation, and its soft X-ray spectrum was extremely steep, modeled by a power-law with photon index more than 4 (Forster & Halpern 1996; Brandt et al. 1999). From an *ASCA* observation Leighly (1999b) found a huge soft excess (which can be described as a black body) in the PHL 1092 spectrum which is 80% of the total flux. An evidence for a line at around 7 keV has also been found and this line could not be explained as an ionized iron line.

Recently Dewangan, & Griffiths (2004) made a detailed study of the XMM-Newton observations of I Zw 1 and they showed that during the X-ray variability the power-law component varied without any change in the soft X-ray excess component. In contrast to this, PHL 1092 shows large variability and it has more than 80% soft X-ray excess component. To understand the X-ray spectral variability of this high luminosity object we have analyzed an *XMM-Newton* observation on this source. We present results based on this observation, including flux selected spectroscopy of high and low flux

<sup>1</sup> Department of Astronomy and Astrophysics, Tata Institute of Fundamental Research, Mumbai-400005, India, email: surajit@tifr.res.in, arrao@tifr.res.in

<sup>2</sup> Department of Physics, Carnegie Mellon University, 5000 Forbes Avenue, Pittsburgh, PA 15213 USA, email: guabrd@cmu.edu

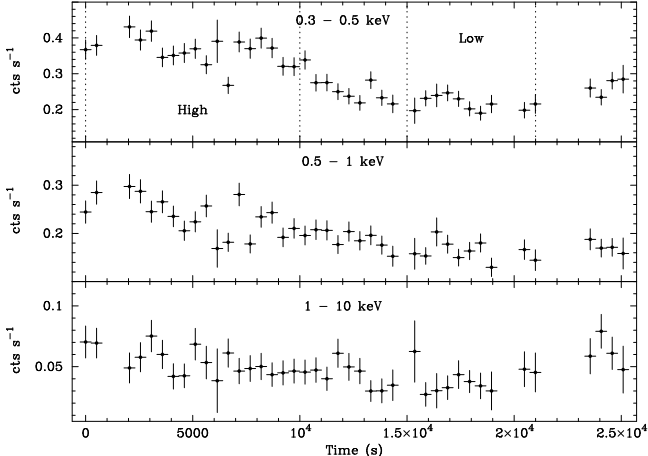


FIG. 1.— PN light curves of PHL 1092 in the  $0.3 - 0.5$  keV (top panel),  $0.5 - 1$  keV (middle panel) and  $1 - 10$  keV (bottom panel) bands with a bin size of 512 s. The high and low flux states used for flux selected spectroscopy are shown by dotted vertical lines in the top panel of the figure.

states.

## 2. OBSERVATION AND DATA REDUCTION

PHL 1092 was observed by *XMM-Newton* observatory on 2003 January 18 using the European Photon Imaging Camera (EPIC) and the reflection grating spectrometer (RGS). The raw events were processed and filtered using the most recent updated calibration database and analysis software (SAS v6.0.0) available in 2004 March. Events in the bad pixels and those adjacent pixels were discarded. Only events with pattern 0 – 4 (single and double) for the PN and 0 – 12 for MOS were selected. Examination of 16 s bin light curve extracted from the full field, excluding the source region, and above 12 keV showed high particle background in some observation intervals. The background flaring region is excluded using the criterion 'rate  $< 3$ ' and minimum good time interval  $> 512$  s for PN data. This resulted in 'good' exposure time of  $\sim 18.9$  ks for the PN. And during these good time intervals the MOS1 and MOS2 background were reasonably low, so we took the same time interval for MOS data also. The net count rate is  $0.53$  counts  $s^{-1}$  in PN and  $0.12$  counts  $s^{-1}$  in MOS1 and MOS2.

## 3. TEMPORAL ANALYSIS

X-ray light curves of PHL 1092 were extracted from the PN and MOS data using a circular region of  $35''$  and  $45''$  respectively centered at the source position and in the two soft bands ( $0.3 - 0.5$  keV and  $0.5 - 1$  keV) as well as in the hard band ( $1 - 10$  keV). The energy bands were chosen to separate approximately the spectral components – a power-law (dominant at high energy) and a soft excess component generally observed from NLS1 galaxies (see Leighly 1999b). Background light curves were extracted from source free regions with the same bin sizes, exposure requirements, as for the source light curves. The area of the region selected for the background is four times the area of the region selected for the source. The background light curves were subtracted from the respective source light curves after appropriate scaling to compensate for the different areas of the extraction regions.

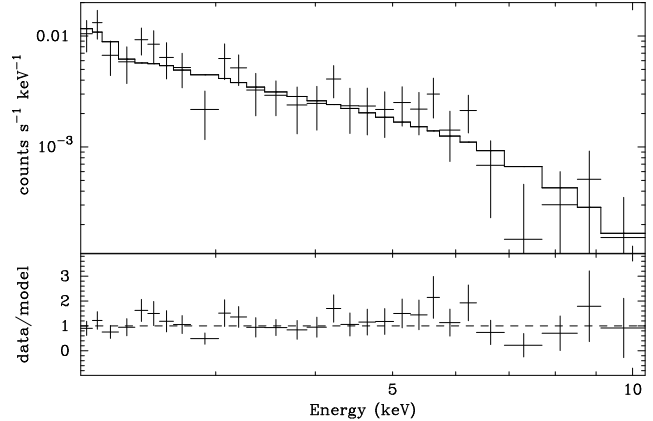


FIG. 2.—  $2 - 10$  keV PN spectrum and best fitted model of absorbed and red-shifted power-law.

Figure 1 shows the PN light curves of PHL 1092 in the different energy bands with a bin size of 512 s. It is evident that X-ray emission from PHL 1092 varied strongly during the *XMM-Newton* observation particularly in the soft bands ( $0.3 - 0.5$  keV and  $0.5 - 1$  keV). There is a sharp decrease in the observed count rates starting from  $10^4$  s (from start of the observation) and reaches a low level in about 5000 s. Two regions are marked as "high" (from start to  $10^4$  s) and "low" ( $1.5 \times 10^4$  s to  $2.1 \times 10^4$  s) in Figure 1 and demarcated by vertical dotted lines. A constant model fit to the complete data gives an unacceptable value for the reduced  $\chi^2$  ( $\sim 7.7$  and  $\sim 3.7$  respectively in the two low energy bands). Fitting constant models to the data in two regions (namely the high-flux state and the low-flux state) gives much lower value of reduced  $\chi^2 \sim 2.2$  and  $\sim 0.73$  respectively in  $0.3 - 0.5$  keV band and  $\sim 2.9$  and  $\sim 0.87$  respectively in the  $0.5 - 1$  keV band. The average count rate throughout the observation in the  $0.3 - 0.5$  keV band is  $0.28 \pm 0.01$   $s^{-1}$ , whereas in the high and low states the average count rates are  $0.36 \pm 0.01$   $s^{-1}$  and  $0.22 \pm 0.01$   $s^{-1}$ , respectively. In the  $0.5 - 1$  keV band the average count rates in the high and low states are  $0.23 \pm 0.01$   $s^{-1}$  and  $0.16 \pm 0.01$   $s^{-1}$ . During the whole observation the average count rate was  $0.19 \pm 0.01$   $s^{-1}$  in this energy band. This shows that the observed count rates varied in a time scale of about 5000 s at a very high significance level. Similarly the average count rate in the  $1 - 10$  keV band is  $0.053 \pm 0.005$   $s^{-1}$  in high flux state and  $0.036 \pm 0.006$   $s^{-1}$  in the low flux state, whereas the average count rate in this band during the whole observation is  $0.047 \pm 0.003$   $s^{-1}$ . So there is a clear variation of count rate in this band too.

## 4. TIME-AVERAGED SPECTRAL ANALYSIS

Photon energy spectra of PHL 1092 and associated background spectra were accumulated from the EPIC PN and MOS data using the source and background extraction method described above. We have also analyzed the RGS data, but the observed count rates are too low to draw any definite conclusion. The source spectra were grouped such that each bin contained at least 15 counts. The EPIC responses were generated using the SAS tasks `rmfgen` and `arfgen`. All the spectral fits were performed with the XSPEC package (version 11.2.0; Arnaud 1996) and using the  $\chi^2$  -statistic. Unless otherwise specified,

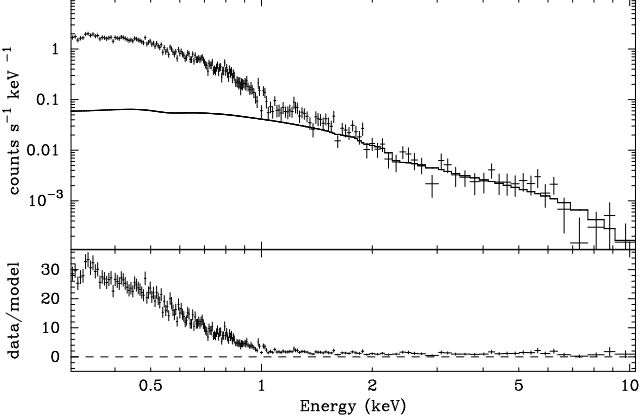


FIG. 3.— The 0.3 – 10 keV EPIC PN spectrum. The extrapolated power-law model is also shown. A strong soft excess is present below  $\sim 2$  keV.

the quoted errors on the best-fit model parameters were calculated for the 90% confidence level for one interesting parameter i.e.,  $\Delta\chi^2 = 2.7$ .

#### 4.1. 2 - 10 keV spectrum

We began studying the spectrum by fitting a red-shifted power-law model with a Galactic  $N_H$  of  $3.53 \times 10^{20}$  (Murphy et. al. 1996) to the EPIC spectrum in the energy range 2 - 10 keV. This provides an acceptable fit giving a photon index  $\Gamma \simeq 1.88$  and a minimum  $\chi^2(dof) = 22(27)$ . The fit to the spectrum and the residuals are shown in Figure 2. There is no clear indication of any line feature near 6 keV. The non-detection of an Iron line is mainly due to the low level of detection significance above 5 keV. The upper limit for the equivalent width of a narrow iron line at 6.4 keV is 289 eV.

#### 4.2. 0.3 - 10 keV spectrum

Extrapolation of the best fitting 2 - 10 keV power law to 0.3 keV shows a huge soft excess in the spectrum (Figure 3). To fit the broad band spectrum, we used one red-shifted blackbody component to parameterize the soft excess. Adding a single blackbody provides a good fit  $\chi^2 \sim 192(196)$  to the soft emission but the power law slope steepens to 2.15. The blackbody temperature is found to be  $\sim 124$  eV. Adding another blackbody gives an improvement with  $\Delta\chi^2 \sim 7$  for two extra parameters and the F-test null probability for adding this component is 0.027. The temperatures of the blackbody components are found to be 129 eV and 53 eV. The data and the folded model are shown in Figure 4. We have also tried using two red-shifted power-law which gives high reduced  $\chi^2$  and is unacceptable.

#### 4.3. PN and MOS data

We have made a joint fit to the PN and MOS data and find that the above model fits the data satisfactorily. The fit and the ratio of data to model are given in Figure 5 and the derived spectral parameters are given in Table 1. The ratio of data to model for the different instruments have been shown separately. In MOS1 there is a slight deficit of counts at around  $\sim 1.4$  keV, whereas in the PN this feature is less significant and in MOS2 this is not present at all. Examining the data to

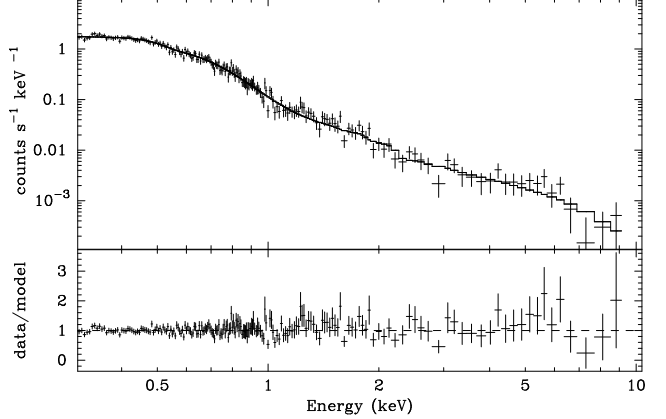


FIG. 4.— PN spectral data and the best-fit model consisting of two absorbed and red-shifted blackbody and a power-law ( $\Gamma \sim 2.1$ ).

model ratio one can argue that there is a slight excess emission at high energies. But we did not get any improvement in the fit by including line or edge parameters at the expected Fe lines and edges. To understand the nature of high energy emission properly we have put several markers (a,b,c,d,e,f) in Figure 5. Markers ‘a’ and ‘b’ are at 7.1 keV and 9.2 keV in the rest frame, respectively (corresponding to neutral and ionized edges of Fe). By examining the data to model ratio at these two energies one can conclude that there is no indication of edge in the data. Markers ‘c’ and ‘d’ correspond to 6.4 keV and 6.9 keV (corresponding to neutral and H-like Fe emission lines), and there is no apparent excess emission at these energies. The apparent line like emission feature in MOS2 data corresponds to unrealistically high energy (marker ‘e’ at energy  $\sim 8$  keV in the rest frame). Again if we consider the edge like feature at high energy in the

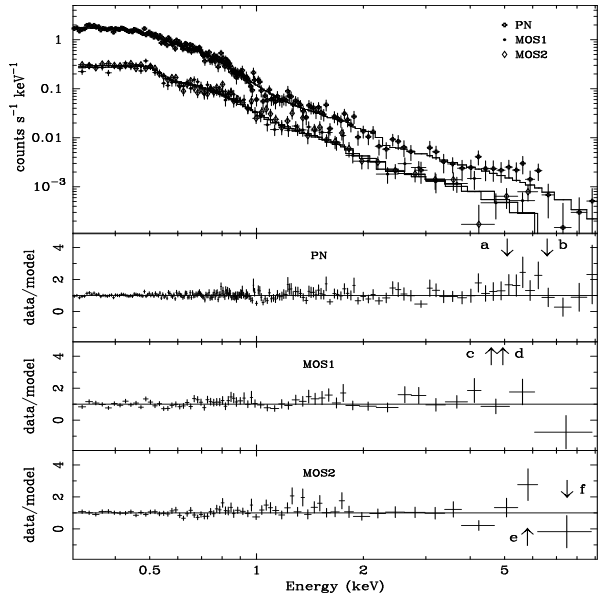


FIG. 5.— PN, MOS1 and MOS2 spectral data and the best-fit model consisting of two absorbed and red-shifted blackbody and power-law ( $\Gamma \sim 2.1$ ) (top panel). Ratio of data to model for PN, MOS1, and MOS2 are also shown separately for clarity. The labels a,b,c,d,e, and f correspond to the source rest frame energies of 7.1 keV, 9.2 keV, 6.4 keV, 6.9 keV, 8 keV and 10.5 keV, respectively (see text).

TABLE 1  
BEST-FIT SPECTRAL PARAMETERS OF PHL 1092.

Component	Parameter	Model <sup>1</sup>		
		PN	PN+MOS	model 2 <sup>1</sup>
Blackbody	$kT$ (eV)	129.0 $^{+3.6}_{-4.4}$	130.1 $^{+3.4}_{-2.8}$	—
	$n_{bb}^2$	6.38 $^{+0.65}_{-1.86}$	6.04 $^{+0.40}_{-0.60}$	—
	$f_{bb}$ (0.3-10 keV) <sup>3</sup>	9.91	9.51	—
Blackbody	$kT$ (eV)	52.8 $^{+13.3}_{-24.5}$	54.3 $^{+3.2}_{-6.5}$	—
	$n_{bb}^3$	13.0 $^{+217.6}_{-11.2}$	13.8 $^{+87.0}_{-9.2}$	—
	$f_{bb}$ (0.3 - 10 keV) <sup>4</sup>	1.12	1.39	—
Power law	$\Gamma$	2.04 $^{+0.21}_{-0.16}$	2.15 $^{+0.13}_{-0.15}$	—
	$n_{pl}^4$	1.19 $^{+0.31}_{-0.19}$	1.37 $^{+0.18}_{-0.19}$	—
	$f_{pl}$ (0.3-10 keV) <sup>3</sup>	2.95	3.06	—
Comptt	$kT_{seed}$ (eV)	—	—	110 $^{+10}_{-12}$
	$kT_{plasma}$ (keV)	—	—	4.8 $^{+12.0}_{-4.1}$
	$\tau$	—	—	0.10 $^{+0.39}_{-0.09}$
Comptt	$n_C^5$	—	—	1.4 $^{+104.2}_{-0.9}$
	$f_C$ (0.3 - 10 keV) <sup>3</sup>	—	—	11.40
	$kT_{seed}$ (eV)	—	—	0.32 $^{+0.25}_{-0.32}$
Comptt	$kT_{plasma}$ (keV)	—	—	59.2 $^{+165.3}_{-57.2}$
	$\tau$	—	—	0.51 $^{+5.05}_{-0.50}$
	$n_C^5$	—	—	0.002 $^{+0.870}_{-0.001}$
Total	$f_{obs}$ (0.3-10 keV) <sup>3</sup>	14.0	14.0	13.6
	$f_{intr}$ (0.3-10 keV) <sup>3</sup>	20.8	20.9	19.9
	$L_{intr}$ (0.3-10 keV) <sup>6</sup>	20.1	20.2	19.2
$\chi^2_{min}/dof$		186/194	334/326	189/191

<sup>1</sup>Parameter values for spectral fits EPIC PN and MOS data. Spectral models were modified by the Galactic absorption. ( $N_H^{Gal} = 3.53 \times 10^{20} \text{ cm}^{-2}$ ). model 1: WABS(BB+BB+PO), model 2: WABS(COMPTT +COMPTT) where WABS: photoelectric absorption, BB: blackbody PO: power-law, COMPTT: Comptonization

<sup>2</sup>Blackbody normalization in units of  $10^{-5} \times 10^{39} \text{ erg s}^{-1}/(d_{10})^2$ , where  $d$  is the distance in the unit of 10 kpc

<sup>3</sup>Flux in the unit of  $10^{-13} \text{ erg cm}^{-2} \text{ s}^{-1}$

<sup>4</sup>Powerlaw normalization in units of  $10^{-4} \text{ photons cm}^{-2} \text{ s}^{-1} \text{ keV}^{-1}$  at 1 keV

<sup>5</sup>Comptonization normalization in units of  $10^{-3} \text{ photons cm}^{-2} \text{ s}^{-1} \text{ keV}^{-1}$

<sup>6</sup>Source luminosity in the unit of  $10^{44} \text{ erg s}^{-1}$

data the corresponding energy will be  $\sim 10.5$  keV (marker ‘f’ in the figure) in the rest frame which is unrealistically high. Hence we can conclude that it is not possible to quantify the high energy excess by these known physical phenomenon. One possible reason of this excess emission at around 8 keV or deficit of counts at around 10.5 keV is an artifact of incorrect background subtraction. In this range background is dominated over the source counts giving rise to an apparent curvature. But if the curvature is true and due to some physical phenomenon then line emission from relativistic ionized accretion disk (laor) cannot be ruled out. By putting a laor line we get an improvement of  $\Delta\chi^2 \sim 8$  (F-test null probability  $\sim 0.2$ ), and the line energy is  $\sim 6.7$  keV in the rest frame (see section 6.4) for five extra parameters.

#### 4.4. Two component thermal Comptonization model

The red-shifted and absorbed blackbodies and power-law model described the data adequately, but the temperature of the blackbodies ( $kT \sim 130$  eV) and ( $kT \sim 50$

eV) are unrealistically high for a standard accretion disk (see section 6.3). A corona with two electron populations with distinct temperatures can give rise to both a soft X-ray excess and a power-law. We investigated if such a process is a viable model for the X-ray spectrum of PHL 1092. The contribution of this soft excess component to the 0.3 – 2 keV band unabsorbed emission is  $\sim 80\%$ . As the temperature of the soft excess component is much higher than that expected from an accretion disk, this component is unlikely to be the intrinsic disk emission. Replacing the soft component by comptt we get a good fit ( $\chi^2 = 190$  for 193 dof). Then we replace the power-law with a hotter comptonized component. The fit is as good as previous ( $\chi^2 = 189$  for 193 dof), since the EPIC instrument cannot determine the value of the electron temperature if  $kT \gtrsim 4$  keV. The exponential roll-over of the comptonized component occurs at  $\sim 4kT$ , and below this point the emission appears as a power-law. Thus if  $4kT$  is very much greater than  $\sim 10$  keV, the temperature cannot be constrained over the XMM-Newton band, and the fit is indistinguishable from a power-law over the same energy range. Because of this the resultant  $\chi^2$  value for the high temperature Comptonization fit is virtually identical with the power-law fit. The parameter values of two comptonization fit are given in Table 1.

#### 5. FLUX-SELECTED SPECTROSCOPY

To investigate whether the flux variability is due to changes of the spectral parameters we have carried out a spectral analysis at low and high flux levels (shown in Figure 1 by dotted vertical lines). We extracted two average spectra covering 0 - 10 ks (high flux state) and 15 - 21 ks (low flux state) in the 0.3 - 10 keV band. The average PN count rates are  $0.64 \pm 0.02 \text{ counts s}^{-1}$  (high flux state) and  $0.41 \pm 0.02 \text{ counts s}^{-1}$  (low flux state). We have used the model (absorbed and red-shifted power-law, and two blackbody) for both the spectra. First we fixed all the parameter previously found values for the combined fit of PN and MOS data and obtained a value of  $\chi^2(\text{dof})$  of 242(141) and 285(85) for the high and low flux data, respectively. These values improved to 165 and 77 when the relative normalization of the two data sets are changed. The fit improved marginally ( $\chi^2(\text{dof})$  of 152(144) and 76(87), respectively) when all the normalizations are allowed to vary mutually. The observed count rates are too low to investigate spectral variability at a greater detail. In Table 2 the fit parameters and the observed fluxes are given. It can be seen from the table that the source is highly variable during the observation. The change in luminosity is  $\sim 35\%$  between the two states.

#### 6. DISCUSSION

This paper presents an analysis of  $\sim 20$  ks *XMM-Newton* observation of the narrow-line QSO PHL 1092. The time-averaged X-ray spectrum of PHL 1092 shows a power-law continuum, a soft X-ray excess described by two red-shifted blackbody components below  $\sim 2$  keV. Above 2.0 keV, the power-law component has a slope of  $\Gamma \sim 2.1$  which is steeper than that of most BLS1 galaxies ( $\Gamma \sim 1.9$ ) but is similar to other NLS1 galaxies e.g, Ton S180 ( $\Gamma = 2.26_{-0.12}^{+0.05}$ ; Vaughan et al. 2002), Mrk 335 ( $\Gamma = 2.29 \pm 0.02$ ; Gondoin et al. 2002), Akn 564

TABLE 2  
BEST-FIT SPECTRAL MODEL PARAMETERS DERIVED FROM THE SPECTRAL FITTING OF THE PN SPECTRA OF PHL 1092.

Component	Parameter	Flux States <sup>1</sup> (high)	Flux States <sup>1</sup> (low)
BB (kT~130 eV)	$n_{bb}^2$	$6.87^{+0.28}_{-0.27}$	$4.59^{+0.43}_{-0.28}$
BB (kT~50 eV)	$n_{bb}^2$	$24.6^{+6.7}_{-6.6}$	$8.9^{+8.3}_{-3.7}$
PO	$n_{pl}^3$	$1.33^{+0.13}_{-0.13}$	$0.74^{+0.74}_{-0.55}$
Total	$f_{obs}$ (0.3-10 keV) <sup>4</sup>	16.01	10.07
	$f_{intr}$ (0.3-10 keV) <sup>4</sup>	24.53	14.91
	$L_{int}$ (0.3-10 keV) <sup>5</sup>	23.64	14.37
	$\chi^2_{min}/dof$	152/144	75/88

<sup>1</sup>High: High flux state; Low: Low flux state

<sup>2</sup>Blackbody normalization in units of  $10^{-5} \times 10^{39}$  erg s<sup>-1</sup>/(d<sub>10</sub>)<sup>2</sup>, where d is the in 10 kpc distance.

<sup>3</sup>Power-law normalization in units of  $10^{-4}$  photons cm<sup>-2</sup> s<sup>-1</sup> keV<sup>-1</sup> at 1 keV.

<sup>4</sup>Flux in units of  $10^{-13}$  erg cm<sup>-2</sup> s<sup>-1</sup>

<sup>5</sup>Source luminosity in units of  $10^{44}$  erg s<sup>-1</sup>

( $\Gamma \simeq 2.50 - 2.55$ ; Vignali et al. 2003). The X-ray continuum steepens at lower energies, resembling the soft X-ray excess emission generally observed from NLS1 galaxies. The strength of this soft X-ray emission is quite high in PHL 1092 compared to other NLS1s. The contribution of the soft X-ray excess emission to the 0.3 – 2 keV band X-ray emission is about 80% in PHL 1092. Such high soft excess has been reported earlier by Leighly (1999b) based on the ASCA data. Variability at similar variability time scale has been reported by Forster & Halpern (1996) based on the ROSAT data.

### 6.1. Black hole mass for PHL 1092

Before we discuss the results in detail, we estimate the mass of the black hole for PHL 1092. Calculations of the black hole mass rely on the assumption that the dynamics of the optical broad-line region gas is dominated by the gravitational potential of the central super-massive black hole. To calculate the black hole mass for PHL 1092, we used the results of Kaspi et al. (2000), based on a reverberation study of 17 quasars. Kaspi et al. (2000) have determined an empirical relationship between the size of the broad-line region ( $R_{BLR}$ ) and the monochromatic luminosity ( $\lambda L_\lambda$ ) as follows.

$$R_{BLR} = (32.9^{+2.0}_{-1.9}) \left[ \frac{\lambda L_\lambda(5100)}{10^{44} \text{ erg s}^{-1}} \right]^{0.700 \pm 0.033} \text{ lt - days} \quad (1)$$

We calculated the flux approximately from the IDS spectrum of PHL 1092 obtained from Bergeron & Kunth (1980) at the rest wavelength of 5100 Å ( $\lambda f_\lambda$  (5100 Å)  $\sim 3 \times 10^{-12}$  erg cm<sup>-2</sup> s<sup>-1</sup>). The mass of the black hole is given by  $M_{BH} = rv^2 G^{-1}$ . To determine  $v$ , the velocity, we correct  $v_{FWHM}$  of the H<sub>β</sub> emission line by a factor of  $\sqrt{3}/2$  to account for velocities in three dimensions. We used  $v_{FWHM} = 1790$  km s<sup>-1</sup> for the H<sub>β</sub> line from Leighly (1999a). The mass is then,

$$M = 1.464 \times 10^5 \left( \frac{R_{BLR}}{\text{lt - days}} \right) \left( \frac{v_{FWHM}}{10^3 \text{ km s}^{-1}} \right)^2 M_\odot \quad (2)$$

Using the cosmology  $q_0 = 0$  and  $H_0 = 50$  km s<sup>-1</sup> Mpc<sup>-1</sup>, this gives us a value for the central black hole mass of  $\sim (1.6 \pm 0.6) \times 10^8 M_\odot$ . Czerny et al. (2001) have reported that the mass of black hole in PHL 1092 is  $1.2 \times 10^6 M_\odot$  from X-ray variability studies and it is  $1.8 \times 10^8 M_\odot$  from accretion disk fitting.

### 6.2. Rapid variability and the efficiency limit

PHL 1092 showed rapid and large amplitude X-ray variability during the *XMM-Newton* observation. X-ray emission from PHL 1092 decreased by  $\sim 35\%$  in 5000 s, corresponding to a change in the 0.3 – 10 keV luminosity of  $\Delta L \sim 10^{45}$  erg s<sup>-1</sup>. This is a remarkable variability for a radio-quiet quasar as the time scale is a factor of  $\sim 10$  shorter than the dynamical time scale for a  $10^8 M_\odot$  Schwarzschild black hole but comparable to the dynamical time scale of Kerr black hole of same mass. Such variability is rare among radio-quiet quasars. Other radio-quiet quasars to show such rapid and large amplitude variability are I Zw 1 (Dewangan, & Griffiths 2004), RX J1334.2+3759 (Dewangan et al. 2002).

The major consequence of rapid and large amplitude variability is that the source has to emit very efficiently. It is possible to calculate the efficiency of conversion of rest mass into energy using simple arguments originally due to Fabian (1979). If the X-ray emitting region is an accreting spherical cloud of ionized hydrogen, then there is a limit on the radiative efficiency,  $\eta$ , given by  $\eta > 4.8 \times 10^{-43} \Delta L / \Delta t$ , where  $\Delta L$  is the change in luminosity in the rest-frame time interval  $\Delta t$ . The change in luminosity between the two states is  $\sim 5 \times 10^{44}$  ergs s<sup>-1</sup> in 5000 s. Assuming uniform and spherical emission this gives a lower limit to the efficiency,  $\eta \gtrsim 0.1$ . This efficiency can be compared with the maximum efficiency possible for a Schwarzschild black hole ( $\eta \simeq 0.06$ ; Shapiro & Teukolsky 1983) and a Kerr black hole ( $\eta \simeq 0.3$ ; Thorne 1974). Thus the rapid variability observed from PHL 1092 is consistent with that expected for a Kerr black hole.

### 6.3. The soft X-ray excess emission

Although the soft X-ray excess emission above a power-law continuum is well described by a blackbody component, its temperature is too high for the intrinsic emission from an accretion disk. There is a relationship between the disk temperature of a standard thin accretion disk, accretion rate and the mass of the black hole, given by (Peterson 1997),

$$T(r) \sim 6.3 \times 10^5 \dot{m}^{1/4} M_8^{-1/4} \left( \frac{r}{r_S} \right)^{-3/4} \text{ K} \quad (3)$$

where  $r_S$  is the Schwarzschild radius, and  $M_8$  is the black hole mass in units of  $10^8 M_\odot$ . The temperature at the last stable orbit ( $r = 3r_S$ ) for a black hole is  $\sim 22$  eV for a black hole mass of  $1.6 \times 10^8 M_\odot$  accreting at the Eddington rate. This is an upper limit to the disk temperature, because  $\dot{m} < 1$ , and outer regions of the disk will have lower temperatures. This can be reconciled by assuming that the low energy excess is due

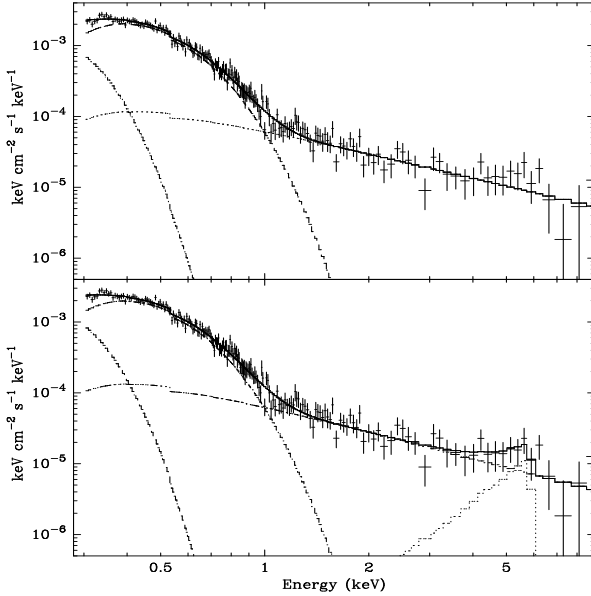


FIG. 6.— Unfolded PN spectral data and best fit model components: two absorbed and red-shifted blackbody and power-law (above) and two absorbed and red-shifted blackbody, power-law and a laor line (below).

to a population of electrons very close to the black hole giving a Comptonized spectrum. In fact the observed X-ray spectrum in the 0.3 - 10 keV region can be fit with a two component Comptonization model. An alternative viable solution is the 'slim disk' (Abramowicz et al. 1988; Chen & Wang 2004, and references therein) which allows temperature higher than the standard disk, and takes place at high accretion rates.

#### 6.4. Possible evidence for a high-energy curvature and absorption

Recently Gallo et. al. (2004) reported a high energy curvature around  $\sim 7$  keV in the same data of PHL 1092. They interpreted the high energy curvature as due to light bending effects very close to the black hole. When we analyze the data using the latest analysis tools (SAS 6.0.0) and latest calibration, we find very little evidence for a high energy curvature and the curvature is centered around 7.5 keV. A narrow Gaussian line cannot give satisfactory fit to the high energy curvature. However a broad Gaussian (width  $\sim 1$  keV) can give an visual improvement of the spectrum (but not statistically significant,  $\Delta\chi^2 \sim 3$  for three extra parameters, F-test null probability  $\sim 0.4$ ) but the line energy becomes greater than 7.2 keV which is clearly unphysical. However a line from a disk around a rotating black hole (Laor 1990) can be used to handle the high energy curvature. The fit is marginally better than the previous fit (see section 4.3). The unfolded spectrum without the Laor line is given in the top panel of Figure 6 and with the line is given in the bottom panel. The line energy is  $\sim 6.7$  keV and the equivalent width is  $\sim 2.5$  keV. Hence we can conclude that Gaussian lines are not required to fit the data, but Laor lines from ionized accretion disk cannot be ruled out. The large equivalent width of the line seems unphysical and in contrast with the fact that the line equivalent width diminishes with increasing continuum luminosity

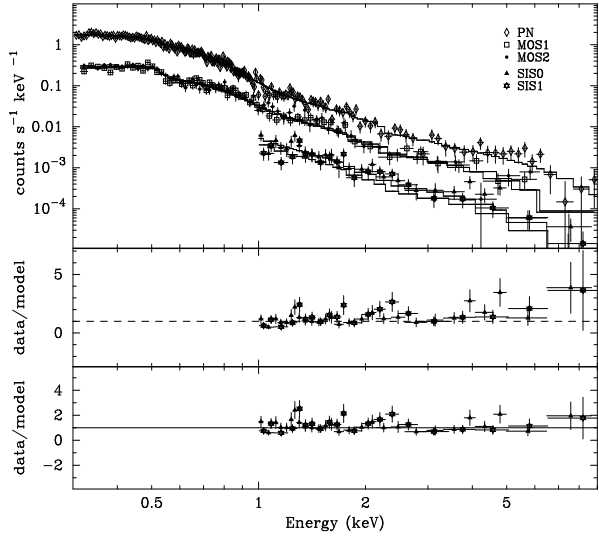


FIG. 7.— PN, MOS1, MOS2, ASCA-SIS0, ASCA-SIS1 spectral data and the best-fit model consisting of two absorbed and redshifted blackbody and power-law (top panel). ASCA-SIS data to model ratio freezing the power-law index of ASCA data to that found in XMM-Newton data (middle panel) and the same model but keeping the value of power-law index of ASCA data free (lower panel). PN, MOS1 and MOS2 data to model ratio have not been shown for clarity.

(Baldwin effect). Gallo et. al. (2004) also reported an absorption line around  $\sim 1.4$  keV. This absorption feature was not present during the 1997 ASCA observation (Leighly 1999b). In section 4.3 we discussed why inclusion of an absorption line or an edge is not feasible. The major reason for the difference in the results given in Gallo et al. (2004) and the present work is the use of most recent calibration and SAS version.

To further understand the high energy spectral shape, we have reanalyzed the ASCA data observed on 1997 July (Leighly 1999a,b). The ASCA-SIS0 and ASCA-SIS1 data are simultaneously fitted with the XMM-Newton EPIC-PN and EPIC-MOS data. To avoid the calibration uncertainties of ASCA-SIS (see ASCA calibration page) below 1 keV we take 1 - 10 keV energy band. We fixed all the parameters obtained from the joint fit of EPIC-PN and EPIC-MOS. The relative normalizations between the instruments are allowed to vary. The relative normalizations of ASCA-SIS0 and ASCA-SIS1 are 1.51 and 1.38 respectively. The fit obtained is quite satisfactory ( $\chi^2 \sim 397$  for 377 dof), indicating that over the different epochs of observation variability can be explained by overall flux variation rather than spectral parameter variation. The observed and fitted spectra are shown in Figure 7, along with residuals (plotted as ratio of the data to the model in the bottom panel of the figure). It can be seen that there is a reasonable agreement between the data and the model. Changing the power-law index improved the fit with a  $\Delta\chi^2$  of 17, with the power-law index changing to 1.73. In this case the high energy excess is even lower (see Figure 7 bottom panel). We can conclude that once the low-energy spectral shape is appropriately modeled, there is no necessity of invoking any high energy curvature. The data quality, however, is insufficient (particularly above 5 keV) to make any definitive statements about other possible

spectral features like edges, reflection features etc.

### 6.5. Comparison with the high-soft state of Galactic black hole sources

All the available data suggest a smooth spectrum with all the spectral features varying at a fast time scale. The time scale of variability, however, corresponds to a physical size (light crossing time) of  $1.5 \times 10^9$  km, which corresponds to only 3 Schwarzschild radius for a  $1.6 \times 10^8 M_\odot$  black hole. Since both the spectral components appear to be varying in this time scale, we can conclude that the X-ray emission arises from very close to a rotating black hole. Such emission mechanism is seen in the high-soft states of Galactic black hole (GBH) binary sources. The accretion disk reaches very close to the black hole and bulk motion near to the black hole can give rise to the observed rapid variability (McClintock & Remillard 2004). The rapid variability observed in PHL 1092 on time scale  $\lesssim 10000$  s can be compared with the millisecond flares observed in GBHs (e.g., Zdziarski & Gierlinski 2004). McHardy et. al. (2004) have compared the variability of NGC 4051 in long and short time scales with that of Cygnus X-1 and have concluded that the X-ray variability in NLS1 galaxies scale better with Cyg X-1 in its high state.

The observed 0.3 - 10 keV X-ray luminosity corresponds to 7% (or 10% after correcting for Galactic absorption) of the Eddington luminosity ( $L_{Edd}$ ). If X-ray luminosity represents a fraction (typically  $\sim 10\%$ ) of bolometric luminosity then the bolometric luminosity of PHL 1092 will be  $\sim L_{Edd}$ . The high-soft states of Galactic black hole sources show a total X-ray luminosity above  $\sim 0.1 L_{Edd}$  (Zdziarski & Gierlinski 2004).

For the fast correlated X-ray variability, we can have the following physical picture. The low energy blackbody arises from a optically thick disk extending up to the last stable orbit of a rotating black hole. Within this radius, matter gets accreted at a supersonic velocity which can produce bulk-motion Comptonisation manifested as the power-law. Non-thermal activity (by the possible magnetic field generated by the equipartition of energy) can generate high energy electrons which would be cooled by Comptonization by the copious amount of low energy photons from the low-energy blackbody emission. This can produce highly saturated Comptonization spectrum modeled as a blackbody in the present work. We invoke the bulk-motion Comptonization model given by Chakrabarti & Titarchuk (1995) to estimate the relevant energetics for such a simplified model. The total luminosity of the  $\sim 50$  eV blackbody corresponds to  $\sim 5.4 \times 10^{45} \text{ ergs s}^{-1}$  which is the expected luminosity from a thick accretion disk extending up to 3

Schwarzschild radius for a  $1.6 \times 10^8 M_\odot$  rotating black hole with 0.2 Eddington accretion rate. The power-law luminosity is about 10% of the total luminosity, which is similar to that seen in Galactic black hole sources in their high state (Zdziarski & Gierlinski 2004). Comparison of the timing and spectral properties of such high luminous NLS1 galaxies with the high soft states of Galactic black hole sources would provide additional handle to constrain such a model.

## 7. CONCLUSIONS

We presented spectral characteristics of the narrow line QSO PHL 1092 based on an *XMM-Newton* observation. The main results are as follows.

1. The 0.3 - 10 keV spectrum of PHL 1092, obtained with XMM-Newton, consists of three intrinsic spectral components, namely a steep ( $\Gamma_X \sim 2.1$ ) primary continuum described by a power-law, a soft X-ray excess component described by two red-shifted blackbody ( $kT \sim 130$  eV and  $kT \sim 50$  eV). Iron fluorescent lines are not detected, primarily due to the low detection level at  $> 6$  keV. The intrinsic photoelectric absorption component is consistent with the Galactic absorption.
2. PHL 1092 showed a significant X-ray variability with changes in the luminosity  $\Delta L \sim 10^{45} \text{ erg s}^{-1}$  on a time scale of  $\sim 5000$  s. The radiative efficiency,  $\eta \gtrsim 0.1$ , inferred from the variability is consistent with X-ray emission outside the last stable orbit around a Kerr black hole.
3. The long (comparing *ASCA* and *XMM-Newton* observation) and short term variability of PHL 1092 can be explained by change in overall normalisation without any spectral changes.
4. The existing data do not require any high energy curvature, but we cannot completely rule out the existence of a red-shifted line from the accretion disk near a fast rotating black hole (Laor line).

This work is based on observations obtained with *XMM-Newton*, an ESA science mission with instruments and contributions directly funded by ESA Member States and the USA (NASA). SD would like to acknowledge the partial support from the Kanwal Rekhi Scholarship of the TIFR Endowment Fund. We thank an anonymous referee for useful comments and suggestions.

## REFERENCES

- Abramowicz, M. A., Czerny, B., Lasota, J. P., & Szuszkiewicz, E. 1985, *ApJ*, 332, 105  
 Arnaud, K. A. et al. 1985, *MNRAS*, 217, 105  
 Arnaud, K. A. 1996, in A.S.P. Conference Series, Astronomical Data Analysis Software and Systems V, 101, ed. George, H., J. & Jeannette, B., 17  
 Ballantyne, D. R., Iwasawa, K., & Fabian, A. C. 2001, *MNRAS*, 323, 506  
 Bergeron, J., & Kunth, D. 1980, *A&A*, 85, L11  
 Bergeron, J., & Kunth, D. 1984, *MNRAS*, 207, 263  
 Boller, T., Brandt, W. N., & Fink, H. 1996, *A&A*, 305, 53  
 Brandt, W. N., Mathur, S., & Elvis, M. 1997, *MNRAS*, 285, L25  
 Brandt, W. N., Boller, T., Fabian, A. C., & Ruszkowski, M. 1999, *MNRAS*, 303, L53  
 Chen, L-H., & Wang, J-M. 2004, *ApJ*, in press  
 Czerny, B., Nikolajuk, M., Piasecki, M., & Kuraszkiewicz, J. 2001, *MNRAS*, 325, 865  
 Chakrabarti, S., & Titarchuk, L. G., 1995 *ApJ*, 455, 623  
 Dewangan, G. C., Singh, K. P., Jones, L. R., McHardy, I. M., Mason, K. O., & Newsam, A. M. 2001, *MNRAS*, 325, 1616  
 Dewangan, G. C. 2002, *ApJ*, 581, L71

- Dewangan, G. C., Boller, T., Singh, K. P., & Leighly, K. M. 2002, *A&A*, 390, 65
- Dewangan, G. C., & Griffiths, R. E. 2004, *ApJ*, submitted
- Fabian, A. C. 1979, in *Royal Society of London Proceedings Series A*, 366, 449
- Forster, K., & Halpern, P. 1996, *ApJ*, 468, 565
- Gallo, L. C., Boller, T., Brandt, W. N., Fabian, A. C., & Grupe, D. 2004, *MNRAS*, Submitted
- Gondoin, P., Orr, A., Lumb, D., & Santos-Lleo, M. 2002, *A&A*, 388, 74
- Kaspi, S., Smith, P. S., Netzer, H., Maoz, D., Jannuzi, B. T., & Giveon, U. 2000, *ApJ*, 533, 631
- Kwan, J., Cheng, F., Fang, L., Zheng, W., & Ge, J. 1995, *ApJ*, 440, 628
- Laor, A. 1990, in *Proceedings of a Workshop Held in Varenna, Iron Line Diagnostics in X-ray Sources, Como, Italy*, eds. Treves, A., Giulio, C. P., & Stella, L., (Berlin Heidelberg New York; Springer-Verlag)
- Leighly, K. M. 1999a, *ApJS*, 125, 297
- Leighly, K. M. 1999b, *ApJS*, 125, 317
- McClintock, J. E., & Remillard, R. A. 2004, 'Compact Stellar X-ray Sources', Chapter 4, eds. W. H. G. Lewin & M. van der, [astro-ph/0306213](http://arxiv.org/abs/astro-ph/0306213)
- McHardy, I. M., Papadakis, I. E., Uttley, P., Page, M. J., & Mason, K. O. 2004, *MNRAS*, 348, 783
- Murphy, E. M., Lockman, F. J., Laor, A., & Elvis, M. 1996, *ApJS*, 105, 369
- Osterbrock, D. E., & Pogge, R. W. 1985, *ApJ*, 297, 166
- Peterson, B. M. 1997, *An Introduction to Active Galactic Nuclei* (First edition; Cambridge University Press)
- Phillips, M. M. 1976, *ApJ*, 208, 37
- Porquet, D., Reeves J. N., O'Brien P., & Brinkmann W. 2004, *A&A*, in press
- Pravdo, S. H., Nugent, J. J., Nousek, J. A., Jensen, K., Wilson, A. S., & Becker, R. H. 1981, *ApJ*, 251, 50, 162
- Shapiro, S. L. & Teukolsky, S. A. 1983, *Black Holes, White Dwarfs and Neutron Stars: The Physics of Compact Objects* (1<sup>st</sup> ed.; New York, Wiley-Interscience)
- Singh, K. P., Garmire, G. P., & Nousek, J. 1985, *ApJ*, 297, 633
- Thorne, K. S. 1974, *ApJ*, 191, 507
- Vaughan, S., Boller, T., Fabian, A. C., Ballantyne, D. R., Brandt, W. N., & Trümper, J. 2002, *MNRAS*, 337, 247
- Vaughan, S., Reeves, J., Warwick, R., & Edelson, R. 1999, *MNRAS*, 309, 113
- Vignali, C., Brandt, W. N., Boller, T., Fabian, A. C., & Vaughan, S. 2003, *ArXiv Astrophysics e-prints*, 10278
- Zdziarski, A. A., & Gierlinski, M., *Progress of Theoretical Physics, Proceeding Supplement*, 2004, in press, [astro-ph/0403683](http://arxiv.org/abs/astro-ph/0403683)